Optics Communications 484 (2021) 126685

Contents lists available at ScienceDirect

Optics Communications

journal homepage: www.elsevier.com/locate/optcom

Alignment of DECam-like large survey telescope for real-time active optics and error analysis

Qichang An [a,*], Xiaoxia Wu [a], Xudong Lin [a], Jianli Wang [a], Tao Chen [a], Jingxu Zhang [a], Hongwen Li [a], Haifeng Cao [a,b], Jing Tang [a,b], Ningxin Guo [a,b], Hongchao Zhao [c]

[a] Changchun Institute of Optics, Fine Mechanics and Physics, Chinese Academy of Sciences, Changchun 130033, China
[b] University of Chinese Academy of Sciences, Beijing 100039, China
[c] School of Physics and Astronomy, Sun Yat-sen University (Zhuhai Campus), Zhuhai 519082, China

ARTICLE INFO

Keywords:
Large survey telescope
Alignment
Active optics
Normalized point source sensitivity

ABSTRACT

To obtain relatively high imaging quality in the whole field of view and simultaneously create petabytes of data with a high signal-to-noise ratio, the alignment requirements for the dark energy camera (DECam)-like wide field active optics survey telescope are strict. Ensuring the real-time alignment of the system is the most important target for the future DECam-like large survey telescope due to the requirement for ellipticity of stellar image across the full field of view is much higher than the traditional telescopes. In such case, the alignment procedure needs to be designed more carefully to consider the large dynamical range and tight residual optical aberration at the same time The error of coarse alignment, influence of camera seeing, error of wavefront sensing, and interaction between the active optics and primary focus assembly and the active optics nonlinear factors, are analyzed by focusing on the DECam-like wide-field active optics survey telescope. Finally, the error of a real time active optics system is analyzed using the normalized point source sensitivity (PSSn). The PSSn of an ideal telescope is 0.9698 and the PSSn of a telescope with an alignment error is 0.8359. This work will be a good guide for the design of future large survey telescopes.

1. Introduction

In the age of big data astronomy, a dark energy camera (DECam)-like wide field active optics survey telescope with a primary focus assembly can collect light with higher efficiency, which is the key to the future development of time domain astronomy [1,2]. The large dark energy survey telescope, which is designed to prove the existence of dark energy and dark matter, is required to possess high imaging quality and low geometric distortion over the whole field of view (FoV) [3]. As a result, its optics system is more sensitive to the misalignment of optical elements. Moreover, this trend is exacerbated by the low stiffness of a large telescope's mount and truss. Therefore, the detector assembly and optical elements of a large wide-field telescope requires the independent and real-time positioning during observation to ensure the acquisition of faint stellar. Thus, an active optics system (AcOS) is required for future large survey telescopes to maximize their observation ability and simultaneously lower the requirements of optical manufacturing and assembling accuracy.

The AcOS is provided with feedback by the wavefront sensing system. The curvature sensor, which is more advanced than other wavefront sensors for large survey active optics telescopes, was proposed by Roddier in 1988 [4]. Its basic principle is that the change in the wavefront curvature at the pupil will cause a corresponding change in the light intensity distribution in the intra and extra focus images. According to the transport of intensity equation (TIE), the wavefront phase is further resolved. The curvature sensors, which align the telescope in real time during the digital sky survey procedure, were used in almost all the large active optics telescopes with a wide field, owing to the telescopes' small F #, tight focal plane space and detector Dewar's refrigeration.

Telescopes with a "slow" optical profile, such as 8 m Very Large Telescope (VLT), are insensitive to the tip/tilt of the secondary mirror. The effect of coma can be effectively avoided by rotating around the pivot points. However, large survey systems require a higher degree of freedom constraint on the secondary mirror due to the off-axis aberration. For example, 1 m Korea Research Institute of Standards and Science(KRISS) system can manually calibrate the relative relationship between primary and secondary mirrors by wavefront of multiple fields of views, and the mean square root of system wavefront is better than $\lambda/5$ ($\lambda = 600$ nm) [5,6]. Merit function regression method is efficient for the alignment control of two-mirror optical systems. What is more, for 2.6 m VST and 2.6 m VISTA telescopes, alignment is also based on analytic expression of two-mirror optical systems.

* Corresponding author.
E-mail address: anjj@mail.ustc.edu.cn (Q. An).

https://doi.org/10.1016/j.optcom.2020.126685
Received 12 August 2020; Received in revised form 19 November 2020; Accepted 6 December 2020
Available online 8 December 2020

Primary focus is the most efficient position to locate survey instruments. DECam is one of the most successful survey instruments/telescopes (Mayall, Large Binocular Telescope, Subaru, etc.) with primary focus assembly (PFA) because of its 1.5° FoV [7–10]. Moreover, one of China's most advanced wide-FoV optics instruments, the Wide Field Survey Telescope, will also be fitted with a PFA in the near future [11]. However, for the primary focus telescope(DECam-like), although it has the advantages of simple system and high optical efficiency, its alignment cannot be expressed analytically. At the same time, the gravity and thermodynamic of the PFA have a direct impact on the collimation of the system.

The requirement for the dynamic range of the system wavefront sensing system can be effectively reduced by coarse alignment, (for the wavefront sensing system, a larger dynamic range means that the measurement resolution will be reduced accordingly). Therefore, the misalignment aberration is firstly controlled to a relative low level (usually tens of microns) by non-optical methods such as coordinate measurement, and then wavefront sensing is used to reach more precise alignment.

In this study, we will use DECam as an example to realize the alignment of the wide field active optics telescope in real time and analyze the associated error. In Section 2, the description of alignment for a DECam-like active optics survey telescope will be presented to the fundamental frame of the AcOS. In Section 3, the Coarse alignment error is analyzed. In Section 4, fine (real-time) alignment error is analyzed. In Section 5, the alignment error is re-presented by PSSn.

2. Description of alignment for a DECam-like active optics survey telescope

A DECam-like telescope refers to a survey telescope with primary focus assembly. The alignment process is divided into two steps, the first is coarse collimate and the second is fine alignment.

The coarse collimate, which makes the curvature sensor available, is performed prior to the observation each night. During the survey, the AcOS will align the telescope in "real time". At every zenith angle, the AcOS will accomplish fine alignment before the observation time shortly after the shutter is open.

Coarse collimate is carried out using a laser tracker, a well-known commercial coordinate measuring machine (CMM) [12]. After coarse collimate, the natural guide stars with appropriate brightness are selected, and defocused images are obtained using a pair of step charge-coupled device cameras (CCDs), which are staggered before and after in a single shot. By detecting the wavefront in multi-FOVs, the telescope will then be aligned by the AcOS in real time. A schematic of the real time active optics for a large survey telescope is shown in Fig. 1. For both the coarse and fine collimate, errors will be introduced. In this study, we will investigate the origin of the errors and how we can reduce them using calculation or calibration.

3. Coarse alignment error analysis

3.1. Coarse alignment error prediction model

In addition to the wavefront sensing system for a closed-loop AcOS, an auxiliary measurement is also required to achieve system collimation. As a widely used CMM, a laser tracker plays an important role in the collimation of optics systems. When we introduced a laser tracker for system coarse alignment prior to observation, it was necessary to establish a precision model to determine whether it was sufficient to determine the position of the elements within the region where the curvature sensor works well. If one laser tracker is insufficient, multiple laser trackers will be combined to break its own precision limit, as done by the Shanghai Institute of Applied Physics for the process of a circular accelerator [12,13].

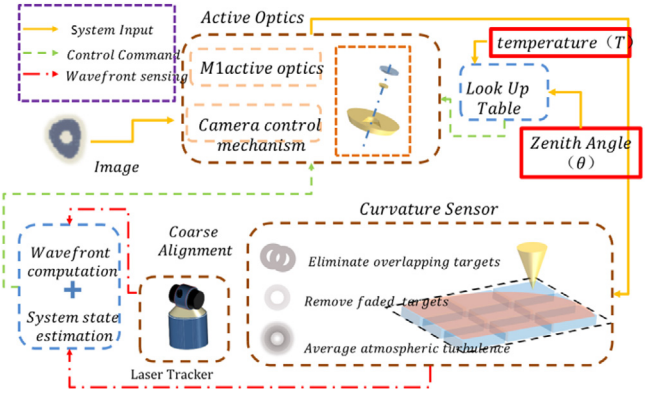

Fig. 1. Schematic of real time AcOS for a large survey telescope (including suppression for star crowding).

Here, at the ith measurement, the ideal measurement vector is:

$$\vec{t}_i = \left(r_i \cos\beta_i \cos\alpha_i, r_i \cos\beta_i \sin\alpha_i, r_i \sin\beta_i\right) \tag{1}$$

Where the error of the distance measurement, r_i of the laser tracker is δr, error of the azimuth measurement α_i is $\delta\alpha$ and error of the altitude measurement β_i is $\delta\beta$.

Using differential calculus, the measurement error at a particular point of the laser tracker is assumed to be

$$\delta^M\vec{t}_i^T = \begin{pmatrix} c\beta_i c\alpha_i & -r_i c\beta_i s\alpha_i & -r_i s\beta_i c\alpha_i \\ c\beta_i s\alpha_i & r_i c\beta_i c\alpha_i & -r_i s\beta_i s\alpha_i \\ s\beta_i & 0 & r_i c\beta_i \end{pmatrix} \begin{pmatrix} \delta r \\ \delta\alpha \\ \delta\beta \end{pmatrix} \tag{2}$$

where c refers to cosine, and s refers to sine. The coarse alignment system for a DECam-like survey telescope with 3–4 m primary mirror is shown in Fig. 2(a). The measurement error of the coarse alignment system is partially dependent on the height of the laser tracker, as shown in Fig. 2(b) and (c). For the error of the azimuth measurement, $\delta\alpha$, and altitude measurement, $\delta\beta$, the root mean square (RMS) is set as 1" and the maximum is set as 3", to estimate the role of the error boundary.

Thus, the location error for the PFA and primary mirror are 50 μm and 20 μm, respectively.

3.2. Model bias estimation and testing

Previously, we assumed that the encoder was uniform without any bias. However, the accumulation of system error and out-of-roundness in the encoders will bias the model. Here, the effect of bias was tested.

According to the characteristics of the alignment procedure (long-range motion followed by small adjustment), the experiments were carried out for long-range and small motion measurements. The precision analysis of the small motion measurement was carried out using a high-precision steward platform, as the reference (the accuracy of which is better than 1 μm), in a "step moving" test, as shown in Fig. 3(a). Furthermore, the long-range measurement precision was realized by repeating measurements with a high-precision metal bar (3-coordinate measurement value 1016.0151 mm) in various positions, as shown in Fig. 3(b).

According to Fig. 3(c), the locating accuracy of the primary mirror was 10 μm, on a small scale.

However, for long-range testing, the error stems from two aspects: one is the error of the length testing and the other is the out-of-roundness of the azimuth axis encoder

In the actual measurement, the out-of-roundness of the azimuth axis encoder will influence the length testing with a SIN-like profile. The same high-precision metal bar is measured at different azimuth

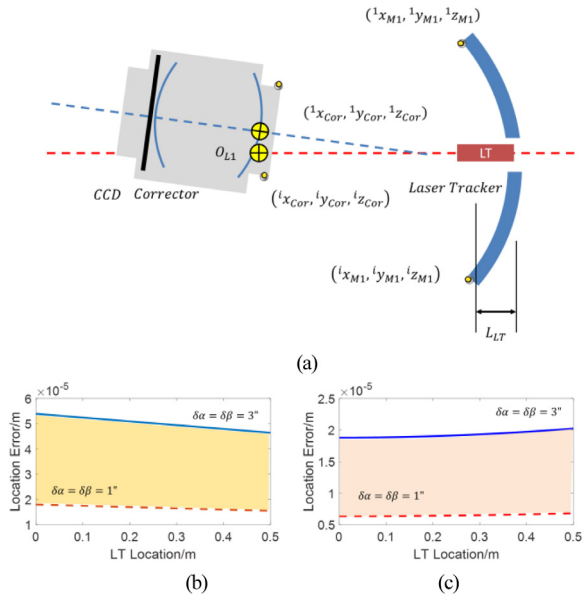

Fig. 2. Measurement error of the coarse alignment system is related to the height of the laser tracker, for (a) showing the height of Laser Tracker, for (b) PFA, and for (c) primary mirror.

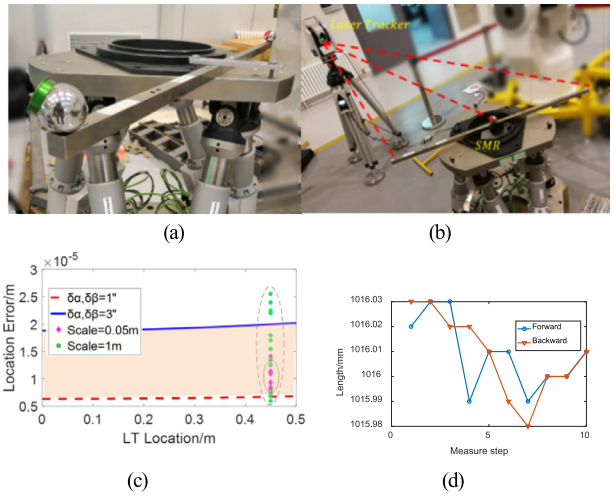

Fig. 3. Precision experiment of laser tracker for (a) experiment site map, (b) measuring the long-range motion and small displacement experiment. (c) Accuracy of measurement and (d) Azimuth axis encoder un-roundness effect.

angles, and the measuring length is shown in Fig. 3(d). The influence is approximately 20 μm at a 90° range.

Thus, the final coarse alignment error for the PFA and the primary mirror are approximately 54 μm and 28 μm, respectively.

4. Fine (real-time) alignment error analysis

When the coarse alignment is close to its precision limit, the system wavefront sensor system can also obtain the measurement result. In this case, the coarse alignment is considered complete and fine adjustment can be made next step.

4.1. Wave front sensing aberration

The wavefront sensing is realized by the curvature sensor and its error primarily originates from:

(a) Error propagation in the solution of the TIE;
(b) Variation of optics aberrations within the wave front sensing FoV;
(c) Mounting error (tip/tilt) of the CCD.

Firstly, a single component sine wavefront phase, $\phi(x) = B\sin(2\pi^f u x)$, is used to calculate the error propagation of the curvature sensing at different spatial frequencies. The relative error of the measurement is shown in the Eq. (3), where ${}^f u$ is the spatial frequency of the sine phase, B is the magnitude of the sine aberration, x is the coordinate on the pupil [13].

$$U(x,0) = Pe^{jB\sin(2\pi^f ux)} \approx P\left[1 + jB\sin\left(2\pi^f ux\right)\right] \tag{3}$$

$$\begin{aligned} &U(x,z) \\ &= \mathcal{F}^{-1}\left\{\mathcal{F}\left\{P\left[1 + jB\sin\left(2\pi^f ux\right)\right]\right\}\exp^{-j\pi\lambda z\eta_x^2}\right\} \\ &= Pe^{j\lambda/2\pi z}\left[1 + jBe^{-j\pi\lambda z^f u^2}\sin\left(2\pi^f ux\right)\right] \end{aligned} \tag{4}$$

The irradiance, $I(x,z)$, is the square of the light field, $U(x,z)$:

$$I(x,z) = |U(x,z)|^2. \tag{5}$$

The differential of the light intensity along the optical axis can be approximate by Eq. (6):

$$\begin{aligned} &I(x,\Delta z) - I(x,-\Delta z) = |U(x,\Delta z)|^2 - |U(x,-\Delta z)|^2 \\ &= 4BI_0\sin\left(\pi\lambda\Delta z^f u^2\right)\sin\left(2\pi^f ux\right) \end{aligned} \tag{6}$$

where, we denote $I_0 = P^2$.

The differential of the light intensity along the optical axis is:

$$\frac{\partial^2 I(x,0)}{\partial z^2} = 2BI_0\pi\lambda^f u^2\sin\left(2\pi^f ux\right) \tag{7}$$

The error propagation is shown in Eq. (8) and we denote $\Delta z = f(f-l)/l$. The relationship between the special frequency and the error propagation is shown in Fig. 4(a).

$$\begin{aligned} \delta &= \left|\frac{\frac{2BI_0\sin(\pi\lambda\Delta z^f u^2)\sin(2\pi^f ux)}{\Delta z} - 2BI_0\pi\lambda^f u^2\sin\left(2\pi^f ux\right)}{2BI_0\pi\lambda^f u^2\sin\left(2\pi^f ux\right)}\right| \times 100\% \\ &= \left|\frac{\frac{2\pi\lambda^f u^2 BI_0\sin(\pi\lambda\Delta z^f u^2)\sin(2\pi^f ux)}{\pi\lambda\Delta z^f u^2} - 2BI_0\pi\lambda^f u^2\sin\left(2\pi^f ux\right)}{2BI_0\pi\lambda^f u^2\sin\left(2\pi^f ux\right)}\right| \times 100\% \\ &= \left|\frac{\pi\lambda^f u^2 BI_0\sin c\left(\pi\lambda\Delta z^f u^2\right)\sin\left(2\pi^f ux\right) - BI_0\pi\lambda^f u^2\sin\left(2\pi^f ux\right)}{BI_0\pi\lambda^f u^2\sin\left(2\pi^f ux\right)}\right| \times 100\% \\ &= \left|\frac{\sin c\left(\pi\lambda\Delta z^f u^2\right) - 1}{1}\right| \times 100\% \end{aligned} \tag{8}$$

Here, the precision of the Curvature Sensor increases with a decrease in spatial frequency. An iterative method should be used to balance the relationship between the increased correction ability and decreased precision. For a real-time AcOS, we want to limit the curvature sensing error to a level of 2% by iterations in 3 times. So that, the initial error is 10 log(2%)/3 = 27%, which is the region is highlighted in Fig. 4(a).

Secondly, the aberration on the wavefront sensing field, for example 0.15°×0.15°, is used as feedback for the AcOS. Thus, the optics aberration tested within this region will be regarded as the center of this FoV. The error introduced by this procedure was analyzed for astigmatism and coma, which are the primary tools used to collimate the telescope.

The coarse alignment can limit the translation and tipping within 54 μm and 0.001°, respectively.

At this point (the very beginning of the fine alignment), the primary aberration (astigmatism and coma) is shown in Fig. 4(b)–(e). The deviation between the averaging and center FoV aberration is less than $\lambda/20$, which is sufficient to facilitate the alignment completely.

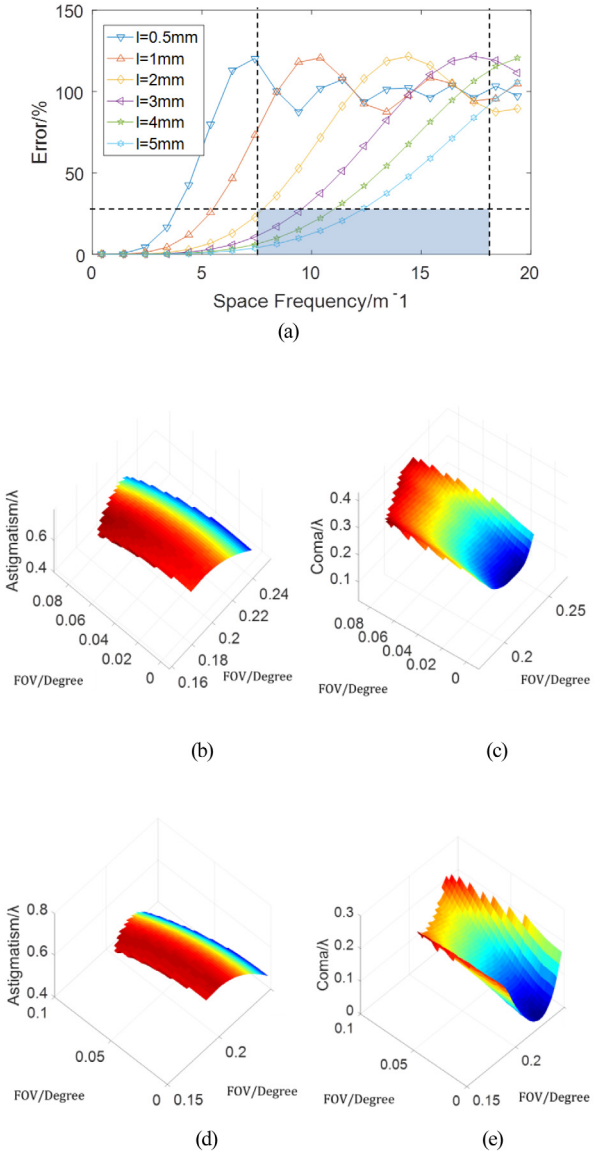

Fig. 4. Fine alignment error analysis for (a) CS error, (b) astigmatism at 0.001° tilting, (c) coma at 0.001° tilting, (d) astigmatism at 50 μm decenter, and (e) coma at 50 μm decenter.

Thirdly, the CCD tipping/tilt will affect the wavefront sensing data, as shown in Fig. 5(a). The influence on the 5-12th Zernike polynomials under tilting (0-0.05°) is shown in Fig. 5(b).

To conclude, the wavefront sensing is not sensitive to tilt within 1”. This can be used to reduce the accuracy of the detector integration, and thus, reducing the equipment cost and assembly time.

4.2. Camera seeing and its estimation

The PFA is placed on the front-end of the telescope. Thus, the atmospheric disturbance around it will influence the wavefront sensing in the AcOS. Here, we define the camera seeing, $seeing_{Cam}$, in Eq. (9)

$$seeing_{Cam} = \left(seeing_{Dom\_Cam}^{5/3} + seeing_{Mirror\_Cam}^{5/3} \right)^{3/5} \tag{9}$$

where $seeing_{Dom\_Cam}$ is the seeing introduced by the layers of air between the dome and camera (PFA), and $seeing_{Mirror\_Cam}$ is the seeing introduced by the layers of air between the primary mirror and PFA.

Considering the Large Synoptic Survey Telescope, which is still in development, as an example [14,15], the light path is required to pass through the camera multiple times. The thermal escape of the camera assembly is approximately 200 W. Therefore, camera thermal control is required to satisfy the image quality in the optical design.

The camera seeing changes as a function of time, temperature, and wind speed, thus, more appropriately specified by actual measurement. Combined with the hypothesis of "frozen turbulence”, the measurement of average slope of the wavefront can estimate the atmospheric turbulence on the light path. As shown in Fig. 7(a) and (b), an autocollimator and guides facilitate the camera seeing test. However, for different wind speeds in natural turbulence, the fans are closed and for forced turbulence, the fans work at maximum power.

In Fig. 6(c)–(d), we can observe that the under wind speed of approximately 5 m/s, the seeing under lab conditions is approximately 0.2”. Thus, the instrument can be allocated on the future DECam-like survey telescope to monitor the camera seeing.

4.3. Interaction between active optics and large lens in PFA

When the PFA is actively positioned in all five axes (focus, centering, and tilt), it also shifts the image in the focal plane, which introduces an interaction between the active optics and pointing.

A DECam-like survey telescope is different from the survey telescope with a relative smaller and lighter second mirror. When the PFA tilts, the correct lens will significantly deflect.

The PFA is tilted by an angle of $\Delta\theta_{Tel}^{X}$ around its peak and f' is the focus length of the telescope. L is the distance from the top end of the PFA to the primary focus of the telescope.

When the PFA tilts around its coma neutral point (CNP), which is fairly close to the prime focus point, the pointing of the telescope will not be influenced.

Thus, we chose the CNP as the pivot point, which is used to analyze the wavefront error. As an example, the RMS is changed by approximately 5 nm for the largest lens.

4.4. Nonlinear influence of alignment model based on sensitivity matrix

The closed-loop AcOS requires an analytical model to link the wavefront error and misalignment. To collimate a 2° FoV off-axis telescope, the sensitivity matrix was introduced by Yang in 2007. By using the wavefront sensing at three FoVs, the system wavefront error reduced to $\lambda/10$ or below [16,17].

Here, we used the results of Yang’s investigation and selected a sensitivity matrix to align the telescopes. The principle of active optical adjustment, using a sensitivity matrix, is shown as follows

$$A\Delta D = \Delta Z \tag{10}$$

where $A = \begin{pmatrix} \frac{\partial a_1}{\partial u_1} & \cdots & \frac{\partial a_1}{\partial u_N} \\ \vdots & \ddots & \vdots \\ \frac{\partial a_m}{\partial u_1} & \cdots & \frac{\partial a_m}{\partial u_N} \end{pmatrix}$ is the sensitivity matrix, $\Delta D = \begin{pmatrix} \delta u_1 \\ \vdots \\ \delta u_N \end{pmatrix}$ is the motion for the executive element, and $\Delta Z = \begin{pmatrix} \delta a_1 \\ \vdots \\ \delta a_N \end{pmatrix}$ is the change of the Zernike polynomial coefficient.

The wavefront errors at corresponding fields, which are introduced by the gravity sag temperature and optical system, are obtained through the curvature sensors. In this case, the linear relationship between the Zernike polynomial coefficient and actuator is not evident. Therefore, multiple iterations are required to obtain the required precision.

The wavefront RMS around all the FoVs, under different PFA decenter misalignments, are shown in Fig. 8(a)–(c).

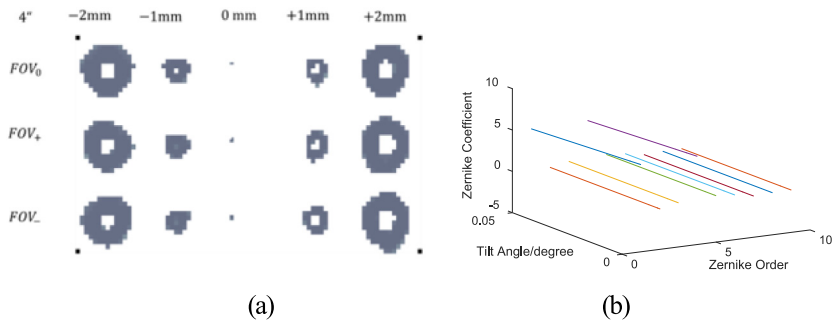

Fig. 5. (a) Influence of detector tilting error for 4" tilt and (b) WS error variation with tipping.

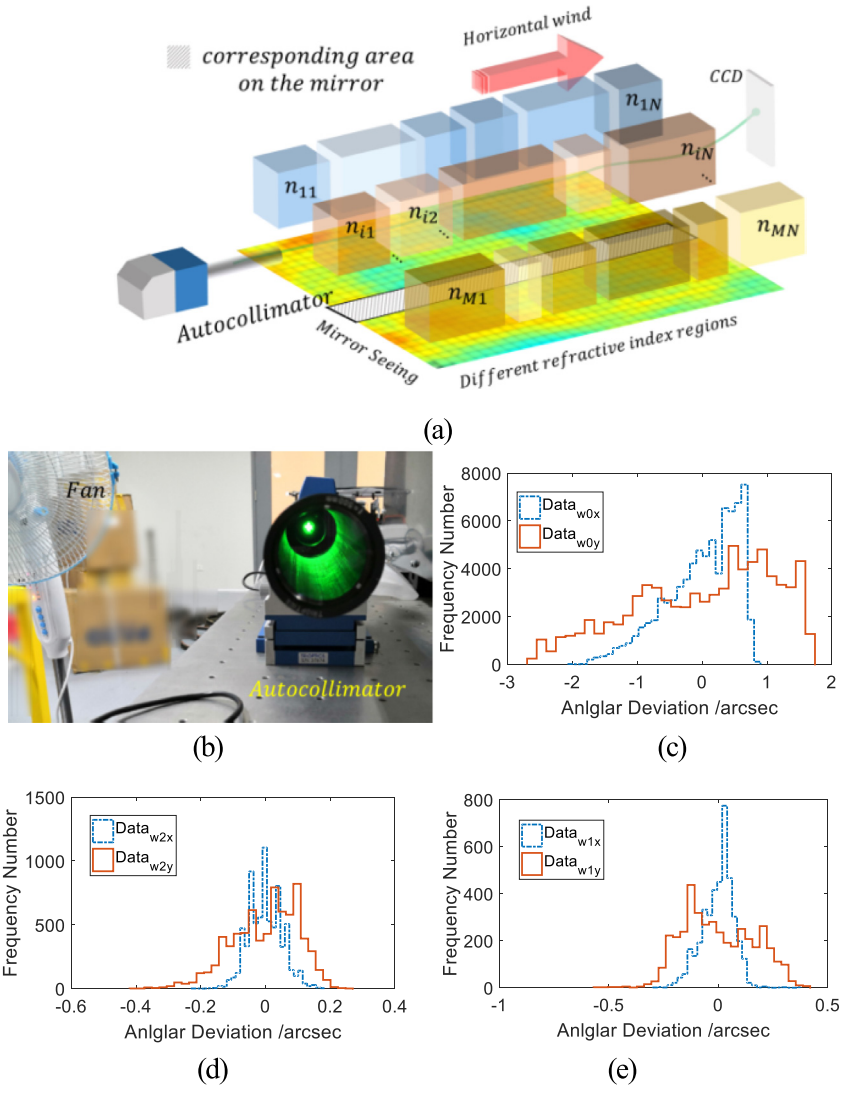

Fig. 6. Configuration of camera seeing test. (a) depicts the basic principles, (b) auto-collimator, (c) natural turbulence, (d) mixed turbulence, and (e) forced turbulence.

As shown in Fig. 8(d), the aberration variation versus the PFA decenter motion step demonstrated that the non-linear characteristics are evident, and the sensitivity matrix for different degrees of optical misalignment is clearly different, especially for a "fast" system (camera, survey telescopes, and so on.).

The residual linearization error is at 70%, if we use the averaging sensitivity (between 0-50 μm) to present the variable sensitivity. Therefore, we require five iterations to limit the error to 5% and ensure that it is within the linear range (in every 10 μm).

5. Error analysis using PSSN

The alignment error will be specified according to the normalized point source sensitivity (PSSn). The PSSn is a new metric for the performance evaluation of large telescopes, first used in the thirty meter telescope [18]:

$$PSSn = \frac{\int |PSF_{t+a+e}(u,\xi)|^2}{\int |PSF_{t+a}(u,\xi)|^2} \tag{11}$$

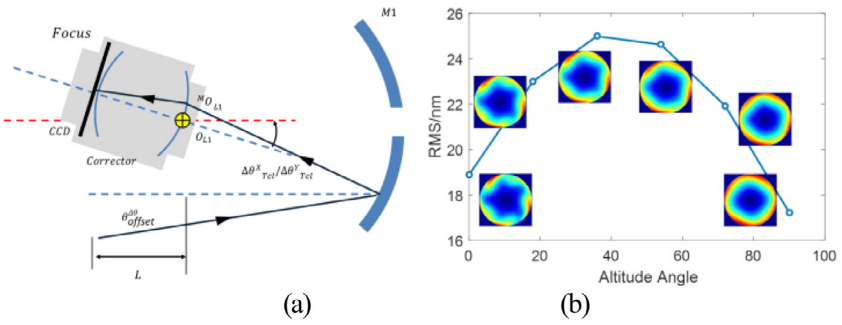

Fig. 7. Influence of detector error on pointing, for (a) decenter and (b) tilt.

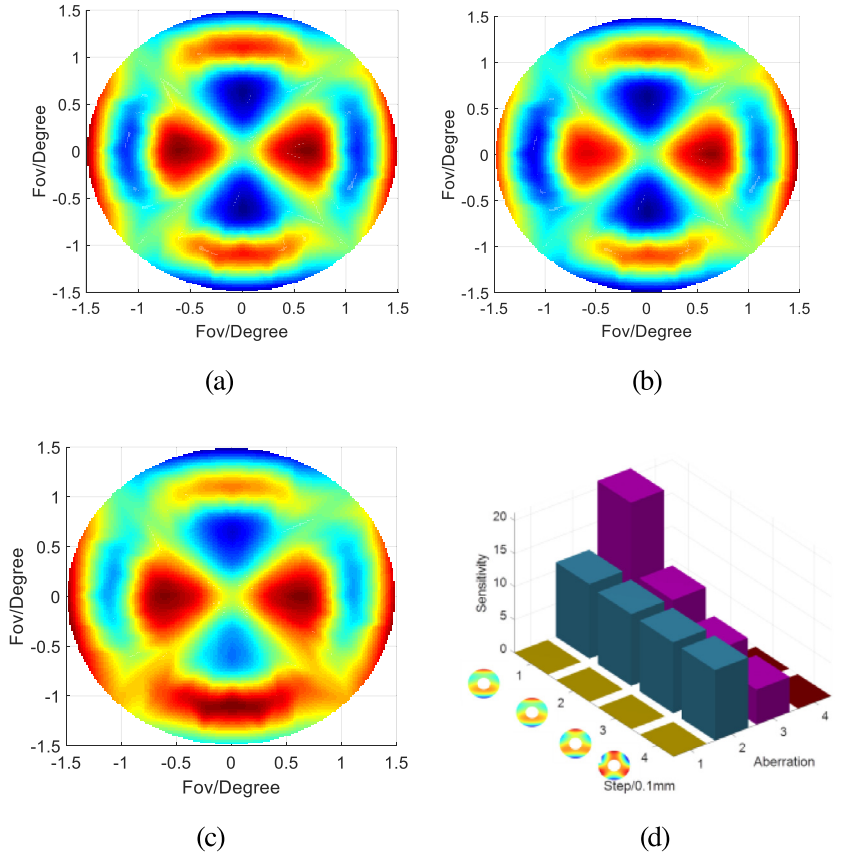

Fig. 8. Configuration of the alignment for (a) 0 μm, (b) 20 μm, and (c) 40 μm. (d) shows the sensitivity matrix for different error values.

$PSF_{t+a+e}(u,\xi)$ is the error coupled Point Spread Function (PSF) of the telescope under seeing on the Fourier plane, (u,ξ), and $PSF_{t+a}(u,\xi)$ is the error-free PSF of the telescope on the Fourier plane, (u,ξ). PSSn overs the whole Fourier plane and links all the environmental and internal factors together. Here, all the errors will be reformed into PSSn and summarized into a final result.

The PSSn of the lens in the PFA at different camera seeing is shown in Fig. 9.

For the previous testing, the camera seeing was set to 0.3", thus, it will influence the PSSn calculation. When the telescope is tracking a star, the tracking error is 1", the atmospheric turbulence over a long time integration is 1.5" (r_0 = 0.068 m), and the Dewar vibration and wind load's influence are estimated to be 0.1" and 0.5", respectively. PSSn of alignment model iteration steps between 0-50 μm, and camera seeing at r0 = 0.068 m is shown in Fig. 10. The interaction of the PFA and AcOS is approximately 0.9998, and the PSSn of five iteration steps is 0.9886.

Here, the approximation of the PSSn though the quadrature sum of full width at half maximum is calculated by Eq. (12) [19,20]. It can release the combination effect of PFA and the camera seeing.

According to the existing literature, a lot of work has been done on frequency domain evaluation methods abroad, especially the error analysis allocation based on PSSn, which has gradually become the mainstream index for each next generation of large aperture telescopes. Through analysis, it can be found that the best PSSn system is 0.8263 (diffraction limit system is 1) under the existing conditions of camera Seeing . It is not only inexpensive to further improve the optical quality of individual links, but also limited to the final image quality improvement of the system.

At the same time, the maximum PSSn of the passive system is 1. However, the PSSn of the active correction system can be greater than 1, or the correction capability of the active optics can be simulated and estimated using PSSn. As shown in Fig. 9, the PSSn of the active optics

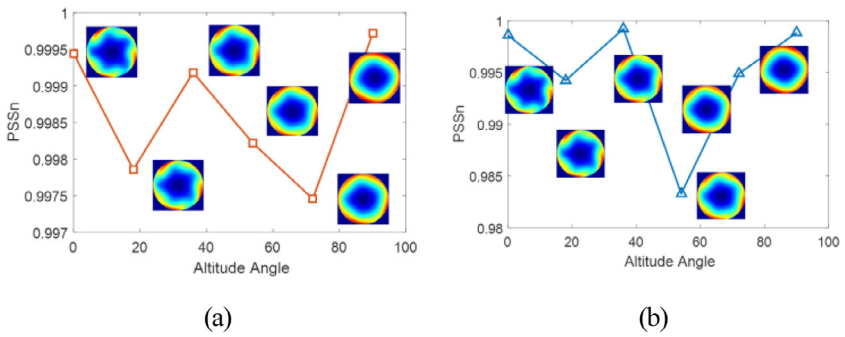

Fig. 9. PSSn of the lens in the PFA at different camera seeing for an alignment of (a) r0 = 0.1 m and (b) r0 = 0.02 m.

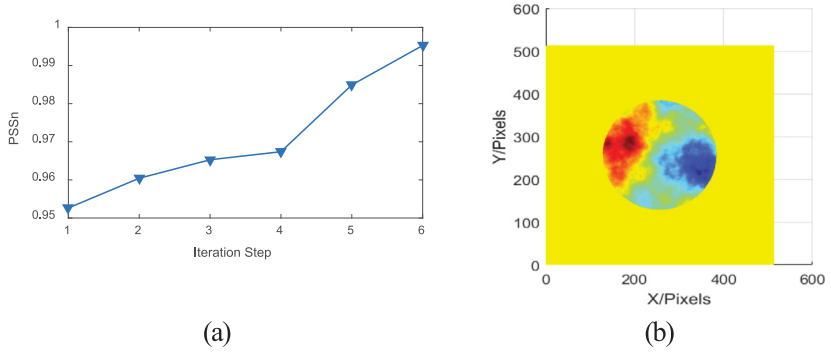

Fig. 10. (a) PSSn of alignment model iteration steps between 0–50 μm. (b) Camera seeing at r0 = 0.068 m.

system is 1.0439.

$$PSSn_{\mathrm{Tel}} = \frac{FWHM_{Cam}^2}{FWHM_{Cam}^2 + \sum_i FWHM_{Tel,i}^2} PSSn_{AcO} = 0.8263 \tag{12}$$

6. Conclusions

For the wavefront sensing system of a large DECam-like survey telescope, a laser tracker is used as the coarse alignment system for the PFA and primary mirror collimation. In this step, the defocusing error of the PFA device is 50 μm, the decenter error is 50 μm and the tilt error is 0.0057°. The curvature sensor is then used for further correction. A misaligned curvature sensor installed in four positions of the FoV, was used for wavefront sensing with the detected FOV being 0.15°, and the distance from the focus being 2 mm. To reduce the influence of noise, the first nine-order fringe Zernike polynomial coefficients of the target view-field points are calculated for all pre- and post-focused star images in the field. The measurement error of the first nine orders of the Zernike polynomial is calculated to be 30%. The adjustment quantity, calculated by curvature sensing, can be fully realized each time. When the measurement error is required to be less than 5%, the iteration number is three. Therefore, after the coarse alignment, approximately five iterative cycles of "curvature sensing–fine tuning–curvature sensing" can be carried out to accomplish the alignment of a large wide-field survey telescope. According to these coefficients and the related theories of computer-aided assembly and adjustment, the defocusing error is first adjusted, and then, the eccentricity and inclination error are adjusted. After three iterations, the alignment of the system can be realized. Furthermore, Look Up Table is used to realize the primary mirror figure correction.

In the further work, this high fidelity error analysis method can be migrated to an end-to-end simulator for the overall AcOS' performances. The Using the analytical active optics model and the alignment can be simulated before the first light to predict the telescope's performance and guide the design of future large survey telescopes.

Declaration of competing interest

The authors declare that they have no known competing financial interests or personal relationships that could have appeared to influence the work reported in this paper.

Acknowledgments

The author is grateful to Dr. Wang for providing his valuable suggestions and help. This work was supported in part by the Youth Innovation Promotion Association CAS (No. 2020221). in part by the NSFC under Grant 11803034., 62005279. in part by the Equipment Development Project of Chinese Academy of Sciences (YJKYQ20200057)

References

[1] B.T. Gansicke, M.R. Schreiber, T.O. Oloza, et al., Accretion of a giant planet onto a white dwarf star, Nature 576 (7785) (2019) 61–64.

[2] Q. Guo, H. Hu, Z. Zheng, et al., Further evidence for a population of dark-matter-deficient dwarf galaxies, Nat. Astronom. 4 (3) (2019) 1–6.

[3] D. Neill, G. Angeli, C. Claver, E. Hileman, J. DeVries, J. Sebag, B. Xin, Overview of the LSST active optics system, in: Modeling, Systems Engineering, and Project Management for Astronomy VI, Vol. 9150, 2014, 91500G1-16.

[4] F. Roddier, Curvature sensing and compensation: a new concept in adaptive optics, Appl. Opt. 27 (7) (1988) 1223–1225.

[5] Regis Tessieres, Analysis for Alignment of Optical Systems, The University of Arizona, 2003.

[6] S. Kim, H.S. Yang, Y.W. Lee, et al., Merit function regression method for efficient alignment control of two-mirror optical systems, Opt. Express 15 (8) (2007) 5059–5068.

[7] A. Roodman, K. Reil, C.J. Davis, Wavefront sensing and the active optics system of the dark energy camera, in: Ground-Based and Airborne Telescopes V, Vol. 9145, 2014, 914516.

[8] M.J. Sholl, C. Bebek, R. Besuner A. Dey, J. Edelstein, P. Jelinsky, M.L. Lampton, M.E. Levi, M. Liang, P. Perry, N. Roe, D. Schlegel, BigBOSS: enabling widefield cosmology on the Mayall Telescope, in: Optical Modeling and Performance Predictions V, Vol. 8127, 2011, 81270D.

[9] E. Giallongo, R. Ragazzoni, A. Grazian A. Baruffolo, G. Beccari, C. De Santis, E. Diolaiti, A. Di Paola, J. Farinato, A. Fontana, S. Gallozzi, F. Gasparo, G. Gentile, R. Green, J. Hill, O. Kuhn, F. Pasian, F. Pedichini, M. Radovich, P. Salinari, R. Smareglia, R. Speziali, V. Testa, D. Thompson, E. Vernet, R.M. Wagne, The performance of the blue prime focus large binocular camera at the large binocular telescope, Astron. Astrophys. 482 (1) (2008) 349–357.

[10] S. Miyazaki, Y. Komiyama, H. Nakaya, et al., HyperSuprime: project overview, in: Ground-Based and Airborne Instrumentation for Astronomy, Vol. 6269, 2006, 62690B1-8.

[11] Z. Lou, M. Liang, D. Yao, et al., Optical design study of the Wide Field Survey Telescope (WFST), in: Advanced Optical Design and Manufacturing Technology and Astronomical Telescopes and Instrumentation, Vol. 10154, 2016, 101542A.

[12] J. Lin, W. Meng, L. Yang, Y. Gao, Y. Zhang, Two-face reciprocal orientation for laser tracker, Opt. Precis. Eng. 25 (10) (2017) 2752–2758.

[13] H. Li, Y. Zhang, R.W. Zhang, et al., Model establishment and error compensation of laser tracker station-transfer, Opt. Precis. Eng. 27 (4) (2019) 771–773.

[14] T. Zhao, Y. Qiao, N. Sun, J. Xie, Surface deformation of theodolite primary mirror under the support system, Chin. Opt. 10 (4) (2017) 477–483.

[15] J. Sebag, K. Vogiatzis, LSST camera heat requirements using CFD and thermal seeing modeling, in: Systems Engineering, and Project Management for Astronomy IV, Vol. 7738, 77380D:1–7.

[16] X. Yang, C. Han, Novel algorithm for computer-aided alignment of wide field of view complex optical system, Key Eng. Mater. 364 (2008) 1066–1071.

[17] E. Oteo, J. Arasa, New strategy for misalignment calculation in optical systems using artificial neural networks, Opt. Eng. 52 (7) (2013) 074105.

[18] F. Yang, Q. An, The evaluation and analysis of mirror seeing based on PSSn, Opt. Precis. Eng. 24 (5) (2016) 979–985.

[19] F. Yang, Q. An, J. Zhang, H. Zhao, P. Guo, H. Jiang, Seeing metrology of large aperture mirror of telescope, Opt. Precis. Eng. 25 (10) (2017) 2572–2579.

[20] G.Z. Angeli, B. Xin, C. Claver, et al., An integrated modeling framework for the Large Synoptic Survey Telescope (LSST), in: Modeling, Systems Engineering, and Project Management for Astronomy VI, Vol. 9911, 2016, 991118:1–20.